AD

MEMORANDUM REPORT ARBRL-MR-03291

(Supersedes IMR No. 712)

A THEORETICAL AND EXPERIMENTAL INVESTIGATION OF A TRANSONIC PROJECTILE FLOW FIELD

Charles J. Nietubicz
James E. Danberg
George R. Inger

July 1983

US ARMY ARMAMENT RESEARCH AND DEVELOPMENT COMMAND
BALLISTIC RESEARCH LABORATORY
ABERDEEN PROVING GROUND, MARYLAND

Approved for public release; distribution unlimited.

REPORT DOCUMENTATION PAGE		READ INSTRUCTIONS BEFORE COMPLETING FORM
1. REPORT NUMBER MEMORANDUM REPORT ARBRL-MR-03291	2. GOVT ACCESSION NO.	3. RECIPIENT'S CATALOG NUMBER
4. TITLE (and Subtitle) A THEORETICAL AND EXPERIMENTAL INVESTIGATION OF A TRANSONIC PROJECTILE FLOW FIELD		5. TYPE OF REPORT & PERIOD COVERED Final
		6. PERFORMING ORG. REPORT NUMBER
7. AUTHOR(s) C.J. Nietubicz, G.R. Inger,* and J.E. Danberg		8. CONTRACT OR GRANT NUMBER(s)
9. PERFORMING ORGANIZATION NAME AND ADDRESS U.S. Army Ballistic Research Laboratory ATTN: DRDAR-BLL Aberdeen Proving Ground, Maryland 21005		10. PROGRAM ELEMENT, PROJECT, TASK AREA & WORK UNIT NUMBERS RDT&E 1L161102AH43
11. CONTROLLING OFFICE NAME AND ADDRESS US Army Armament Research & Development Command US Army Ballistic Research Laboratory (DRDAR-BLA-S) Aberdeen Proving Ground, MD 21005		12. REPORT DATE July 1983
		13. NUMBER OF PAGES 32
14. MONITORING AGENCY NAME & ADDRESS(if different from Controlling Office)		15. SECURITY CLASS. (of this report) Unclassified
		15a. DECLASSIFICATION/DOWNGRADING SCHEDULE

16. DISTRIBUTION STATEMENT (of this Report)

Approved for public release, distribution unlimited.

17. DISTRIBUTION STATEMENT (of the abstract entered in Block 20, if different from Report)

18. SUPPLEMENTARY NOTES

This report supersedes IMR No. 712

*Dr. George R. Inger
Associate Chairman, Dept. of Mech. & Aerospace Engr.
West Virginia University
Morgantown, W. VA 26506

19. KEY WORDS (Continue on reverse side if necessary and identify by block number)

Transonic Flow
Projectiles
Velocity Profiles
Navier-Stokes Equations

Shock Boundary Layer Interaction
Computations
Experimental Data

20. ABSTRACT (Continue on reverse side if necessary and identify by block number)

The transonic flow field about a secant-ogive-cylinder-boattail with a turbulent boundary layer has been studied. A joint theoretical and experiment effort is presented which compares the results of a generalized axisymmetric Navier-Stokes code, a composite inviscid boundary-layer/shock interaction solution method, and experiment. The experimental longitudinal pressure distribution at M = 0.94, and 0.97 for α = 0.0° are generally well predicted by both theoretical techniques although the Navier-Stokes solutions are shown to be superior in describing the details, such as, upstream effects of expansion

DD FORM 1473 1 JAN 73   EDITION OF 1 NOV 65 IS OBSOLETE

20. ABSTRACT (Continued)

corners and the position and magnitude of minimum pressure regions. Both theo-
retical solutions predict the boundary layer velocity profiles very well in all
cases with the largest differences occurring just downstream of the boattail
corner. Comparisons of displacement thickness and skin friction distributions
are also presented.

TABLE OF CONTENTS

3

LIST OF ILLUSTRATIONS

I. INTRODUCTION

The aerodynamic characteristics of standard artillery shell from subsonic to supersonic speeds are of major concern in the design of new shell or modifications to existing ones. The possibility that a given shape may have to operate throughout a range of Mach numbers requires a detailed understanding of the flow fields associated with each Mach number. Modern computational techniques are now being applied to projectile shapes and the ability to compute the aerodynamics of shell for a wide range of Mach numbers and Reynolds numbers is becoming a reality. Significant accomplishments have been made in the supersonic regime where static and Magnus force coefficients have been computed for standard projectile configurations; computations compare well with experimental data.[1,2] Transonic flow, however, presents additional complexity for computational analysis. Figure 1 is a Schlieren photo which shows the shock pattern existing about a typical projectile shape at transonic velocity. The formation of shock waves, imbedded in the flow field near the surface discontinuities, produces a severe change in the aerodynamic coefficients such as drag and pitching moment. For example, the drag for a projectile shape has been found to change by as much as 100% through a Mach number range of 0.95 to 0.97.[3] A change of this magnitude in the aerodynamics makes it essential to be able to understand and compute the features of the flow field which contribute to this effect.

A concentrated theoretical and experimental research program has been ongoing at the U.S. Army Ballistic Research Laboratory in order to develop the predictive capabilities required for determining projectile aerodynamics. Supersonic computations using combined inviscid flow field and boundary layer techniques have been developed by Sturek,[1] et al., for cone-cylinder and ogive-cylinder configurations. Recent results have been obtained in supersonic flow over a typical boattailed projectile by Schiff and Sturek[2] using modern computational techniques for solving the parabolized thin-layer Navier-Stokes equations.

1. Sturek, W.B., et al., "Computations of Magnus Effects for a Yawed, Spinning Body of Revolution," AIAA Journal, Vol. 16, No. 7, July 1978, pp. 687-692.

2. Schiff, L.B., and Sturek, W.B., "Numerical Simulation of Steady Supersonic Flow Over an Ogive-Cylinder-Boattail Body," AIAA Paper No. 80-0066, January 14-16, 1980.

3. Nietubicz, C.J., "Navier-Stokes Computations for Conventional and Hollow Projectile Shapes at Transonic Velocities," AIAA Paper No. 81-1262, AIAA 14th Fluid and Plasma Dynamics Conference, Palo Alto, CA, 1981.

Inviscid transonic computational results have been obtained by Reklis,[4] et al., for a secant-ogive-cylinder-boattail shape. This work was then extended to include the viscous boundary layer and modeling of the shock boundary layer interaction regions. A comparison of the composite solution technique with experimental data[5] showed generally good agreement.

A series of 3D computations solving the thin-layer Navier-Stokes equations have been reported by Deiwert[6] for simulating afterbody flow fields. This excellent work was performed on the ILLIAC IV and allowed sufficient grid resolution in the boattail region to show the complicated flow field structure which exists at angle of attack. The availability of these new computational techniques for solving the thin-layer generalized axisymmetric Navier-Stokes equations and additional experimental data has resulted in a continued analysis of this transonic flow field problem. A discussion of the Navier-Stokes and Composite computational methods and available experimental data follows.

II. GENERALIZED AXISYMMETRIC TECHNIQUE

The Navier-Stokes code which has been used in this study is the η-invariant or Generalized Axisymmetric version.[7] This code solves the thin-layer Navier-Stokes equations which are cast in strong conservation law form. The equation formulation allows for arbitrary body geometries and is solved using an implicit, approximate factorization, finite difference scheme. The "thin-layer" approximation[8-9] used here requires that all body surfaces be

4. Reklis, R.P., Sturek, W.B., and Bailey, F.L., "Computation of Transonic Flow Past Projectiles at Angle of Attack," U.S. Army Ballistic Research Laboratory, ARRADCOM, Aberdeen Proving Ground, MD, Technical Report ARBRL-TR-02139, February 1979 (AD A069106).

5. Danberg, J.E., Reklis, R.P., and Inger, G.R., "Pressure Distributions and Boundary Layer Profiles on a Yawed Projectile at Transonic Speeds," University of Delaware Tech Report No. 226, Department of Mechanical and Aerospace Engineering, April 1979.

6. Deiwert, G.S., "Numerical Simulation of Three-Dimensional Boattail Afterbody Flow Field," AIAA Paper No. 80-1347, July 1980.

7. Nietubicz, C.J., Pulliam, T.H., and Steger, J.L., "Numerical Solution of the Azimuthal-Invariant Thin-Layer Navier-Stokes Equations," AIAA Journal Vol. 18, No. 12, December 1980, pp. 1411-1412.

8. Pulliam, T.H., and Steger, J.L., "On Implicit Finite-Difference Simulations of Three-Dimensional Flow," AIAA Journal, Vol. 18, No. 2, February 1980, pp. 159-167.

9. Baldwin, B.S., and Lomax, H., "Thin Layer Approximation and Algebraic Model for Separated Turbulent Flows," AIAA Paper No. 78-257, January 1978.

mapped onto ζ = constant planes and that Re $\gg$ 1. Essentially, all the viscous terms in the coordinate directions (here taken as ξ and η) along the body surface are neglected while terms in the ζ or the near normal direction to the body are retained. This approximation is used because, due to computer speed and storage limitations, fine grid spacing can only be provided in one coordinate direction (usually taken as the near normal direction) and the grid spacing available in the other two directions is usually too coarse to resolve the viscous terms.

The thin-layer generalized axisymmetric Navier-Stokes equations are obtained from the three-dimensional equations by making use of two restrictions: (1) All body geometries are of an axisymmetric type. (2) The state variables and the contravariant velocities do not vary in the circumferential direction. Given the above assumptions the transformed generalized thin-layer Navier-Stokes equations in nondimensional and strong conservation law form are written as[7]

$$\delta_\tau \hat{q} + \delta_\xi \hat{E} + \delta_\zeta \hat{G} + \hat{H} = Re^{-1} \, \delta_\zeta \hat{S} \qquad (1)$$

where general coordinate transformations

$$\xi = \xi(x,y,z,t) \quad - \quad \text{longitudinal coordinate}$$

$$\zeta = \zeta(x,y,z,t) \quad - \quad \text{near normal coordinate}$$

$$\tau = t \qquad\qquad - \quad \text{time}$$

are used.

The vector $\hat{q}$ contains the dependent variables density, ρ, velocity components, u, v, and w, and total energy, e. The vectors $\hat{E}$, $\hat{G}$ and $\hat{H}$ contain terms arising from the continuity equation, three momentum equations and energy equation. All viscous terms are contained in the vector $\hat{S}$. The turbulence modeling used is the two layer Cebeci type eddy viscosity model as modified and reported by Baldwin and Lomax[9]

Equation (1) contains only two spatial derivatives but does retain all three momentum equations, thus allowing a degree of generality over the standard axisymmetric equations. In particular, the circumferential velocity is not assumed to be zero, allowing computations for spinning projectiles or swirl flow to be accomplished.

The numerical algorithm used for Equation (1) is a fully implicit, approximately factored, finite difference scheme as analyzed by Beam and Warming[10] The details of the numerical method, algorithm, and boundary

---

10. Beam, R., and Warming, R.F., "An Implicit Factored Scheme for the Compressible Navier-Stokes Equations," AIAA Paper No. 77-645, June 1977.

conditions can be found in Reference 7. The experiment was conducted in a continuous flow tunnel and thus an adabatic wall boundary condition was used.

The numerical grid used for all the Navier-Stokes computations was generated using an elliptic solver[11] and is shown in Figure 2. The computational region has been extended to four model lengths in front of and four model lengths behind the projectile. The far field boundary has been set at five model lengths. Such an extensive domain is used to eliminate the possibility of any wave reflection back onto the model. The dark band of lines near the model surface results from a clustering of grid lines which are required in order to adequately resolve the boundary layer region. The minimum spacing at the wall was .0002 model diameter, which resulted in at least 3-5 grid points being in the laminar sublayer. The total number of points in the normal direction was 40. There were 78 grid points in the longitudinal direction with clustering taking place at X/D = 3.2 and 5.3, the ogive-cylinder and cylinder-boattail junctions, respectively. No special clustering was applied to the shock boundary layer interaction region.

The projectile base was modeled as an extention of the 7.0° boattail for a distance of two calibers. The surface line was then turned parallel to the model axis for the remainder of the wake area. The base flow is thus modeled as an extended sting. A review of free-flight shadowgraphs for projectile shapes at transonic speeds does show the wake flow to follow near the boattail angle for a distance of one to three calibers before turning parallel to the flow direction.

III. COMPOSITE INVISCID FLOW-BOUNDARY LAYER-SHOCK INTERACTION MODEL-INVISCID FLOW REGION

Inviscid flow calculations were made by methods developed by Reklis, Sturek, and Bailey[4] involving a numerical solution of the transonic small disturbance equation for the velocity perturbation potential ϕ which in cylindrical coordinates is,

$$[(1-M^2) - M^2 (\gamma+1)\phi_x]\phi_{xx} + \phi_{rr} + \phi_r/r + \phi_{\theta\theta}/r^2 = 0 \qquad (2)$$

where M_∞ is the free-stream Mach number and γ is the ratio of specific heats. The coordinates and ϕ are nondimensionalized by the free-stream velocity and a characteristic dimension of the body. This equation is a second order nonlinear partial differential equation of mixed elliptic-hyperbolic type. The type of the equation changes to match the physical differences between regions of subsonic and supersonic flow.

---

11. *Steger, J.L., Nietubicz, C.J., and Heavey, K.R., "A General Curvilinear Grid Generation Program for Projectile Configurations," ARBRL-MR-03142, U.S. Army Ballistic Research Laboratory, ARRADCOM, Aberdeen Proving Ground, MD 21005, March 1982 (AD A107334).*

Equation (2) generally yields adequate predictions of the inviscid flow about a projectile shape such as that studied here. Certain regions of the flow, however, require some modeling. The wake is simulated by a necked-down extension from the boattail base smoothly-fared into a cylindrical sting over a distance of two calbiers; the base flow is thus modeled as an extended sting similar to the Navier-Stokes computations. Of course, the slip surface which physically exists is thus not accounted for in the calculations. Moreover, this obviously fails to account for the wake momentum defect and hence the base contribution to the overall drag. Additionally, there is a slight over-estimation of the pressure rise and hence the boundary layer thickness growth and skin friction drop near the end of the boattail due to neglect of the correct base pressure upstream influence. However, for the present purposes where drag prediction is not of primary interest, these shortcomings are not deemed to be significant.

In order to develop a "conservative" algorithm to solve this equation special care must also be taken at transitions between subsonic and supersonic flow. Nonconservative forms of the algorithm, however, often give better agreement with experiment because the breakdown in conservation approximates the effect of shock obliquity resulting from shock-boundary layer interaction. (See Eq. 3.) The algorithm used here was therefore a nonconservative one for the purposes of providing a first order composite flow model. Consistently, first order boundary condition relations have been used with 120 streamwise grid points along the body length with higher concentration in the corner and shock regions.

IV. BOUNDARY LAYER REGION

Boundary layer flow computations developed for laminar cone flows by Dwyer and Sanders[12] were extended to more general turbulent flows by Sturek,[1] et al. In this technique the boundary layer equations for the conservation of mass, momentum, and energy are solved with an implicit finite difference technique. The solution begins with the development of an approximate boundary layer profile at the tip. The solution is then marched over the body from nose to tail. At each step along the way a two-point boundary value system is solved with conditions given at the body surface and at the boundary layer edge. The possibility of body spin is accounted for and care is taken in setting up the difference equations to maintain stability. Turbulence is accounted for by use of an algebraic type, eddy viscosity, turbulent shear stress model with Van Driest damping. This model has proved suitable for use in cases of supersonic flow and is carried over directly to the transonic regime.

---

12. Dwyer, H.A., and Sanders, B.R., "Magnus Forces on Spinning Supersonic Cones. Part I. The Boundary Layer," AIAA Journal, Vol. 14, April 1976, p. 498.

V. LOCAL SHOCK-BOUNDARY LAYER INTERACTION REGION

For nonseparating interactions (local Mach number roughly less than 1.3) in the Reynolds number range $Re_L \sim 10^6$ to 10^8 a nonasymptotic triple-deck small disturbance solution[13] of the weak normal shock-turbulent interaction is employed. This model has proven very successful in treating transonic interaction on supercritical airfoils including extensive experimental verification;[14] its use therefore provides a sound treatment of both the local and downstream effects while avoiding the use of crude empirical "viscous wedge" models whose fundamental dependence on the incoming boundary layer properties is unknown.

The flow model (Figure 3) consists of a double-decked region of mixed transonic inviscid rotational flow surrounding a shock discontinuity and an underlying thin shear stress disturbance sublayer within the Law of the Wall region that contains the upstream influence and skin friction perturbations. An approximate analytic solution is achieved by assuming small linearized disturbances ahead of and behind the nonlinear shock jump, with a simplified treatment of the detailed shock structure within the boundary layer down to the sonic level. The resulting equations can be solved by operational methods to obtain the interactive pressure rise, displacement thickness growth, and local skin friction solution both upstream and downstream of the shock foot. (See Reference 13 for details.) This solution has been adapted to the present problem by an appropriate extension of the theory that considers the additional terms and effects due to the axisymmetric geometry.[15]

This interaction solution is used as a locally-imbedded "interactive module" astride each of the two shock locations. The presence of a local compression shock abruptly terminating the local pockets of supersonic flow following both body corners is identified and located by the inviscid solution code and used to call the interaction solution as an interruptive subroutine centered about each such shock location, using the appropriate local pre-shock Mach number from the code as a driving input to the solution. When inserting the interaction we account for the fact that the nonconservative inviscid code gives shock strengths slightly less than the full Rankine-Hugoniot normal

---

13. Inger, G.R., "Upstream Influence and Skin Friction of Non-Separating Shock-Turbulent Boundary Layer Interaction," AIAA Paper 80-1411, Snowmass, CO, July 1980.

14. Stanewsky, E., Nanandan, M., and Inger, G.R., "Computation of Transonic Flow on Supercritical Airfoils with a Special Solution for Shock-Boundary Layer Interaction," in AGARD CP-291 ("Computation of Viscous-Inviscid Interactions"), September 1980.

15. Inger, G.R., "Transonic Shock-Turbulent Boundary Layer Interactions on Spinning Axisymmetric Bodies at Zero Angle of Attack," ARBRL-TR-02458, U.S. Army Ballistic Research Laboratory, ARRADCOM, Aberdeen Proving Ground, MD 21005, January 1983 (AD A123389).

shock jump assumed in the interaction solution. The pre-shock Mach number M_1 used in the latter solution is corrected to the value pertaining to a slightly oblique attached shock that produces maximum post-shock flow deflection. This method, which is strongly supported by an interpretation of experimental evidence by numerous investigators (e.g., References 14 and 16), yields

$$M_{1_{eff}} \simeq M_1 \sin(90 - 37.8 \sqrt{M_1 - 1}) \qquad (3)$$

The required inputs from the boundary layer code are the local incoming displacement thickness and shape factor. The interaction subroutine replaces the boundary layer code over the range of the interaction with a complete description (if desired) of the wall pressure, displacement thickness and skin friction, plus the post-interaction values of δ^*, C_f and the (subsonic) inviscid edge conditions needed to re-start the turbulent boundary layer code. This method of introducing the interactive solution allows us to account not only for the rapid displacement thickness growth but also for the attendant distortion of both the skin friction and profile shape. Moreover, the important influence of these changes on the subsequent boundary layer development is included in the post-interaction reinitialization of the boundary layer calculation. Consistent with the turbulent boundary layer model employed within the interaction theory, this reinitialization is carried out at the first station after the interaction by means of the compressible version of Walz's general composite Law of the Wall - Law of the Wake velocity profile model.[17] The profile parameters are chosen to match final values of δ^*, C_f and M_e given by the local interaction solution while the wake function (hence shape factor) automatically takes its consequent highly nonequilibrium post-shock value. Given this starting profile, the turbulent boundary layer code then marches downstream.

It is noted that since the shock locations here are essentially fixed by the sharp corners on the body and were found to alter only slightly due to viscous effects, there is no need to carry out a global interaction for their position as would be the case for supercritical airfoils; that is, to the present first order approximation the shock strength and position may be taken from the inviscid calculation without the displacement thickness effect.

16. Murman, E.M., and Cole, J.D., "Calculation of Plane Steady Transonic Flow," AIAA Journal, Vol. 9, No. 1, January 1971, pp. 114-121.

17. Walz, A., "Boundary Layers of Flow and Temperature," M.I.T. Press, Cambridge, MA, 1969, p. 113.

VI. EXPERIMENT

The experimental data to be described here are an extension of the data base reported at the 12th AIAA Fluid and Plasma Dynamics Conference[18] including new tests at additional survey stations and at Mach number 0.97 as well as the previous reported data at Mach = 0.94.

The wind tunnel measurements were performed in the NASA Langley Research Center 8 foot Transonic Pressure Tunnel (TPT). The tunnel was operated at one atmosphere supply pressure (101.3kPa) and at supply temperature of 49.2°C which resulted in a Reynolds number of 13×10^6 1/M. The TPT facility is of slotted wall construction to minimize reflected wave interference effects which were monitored using tunnel wall static pressure taps. The model was sting mounted from the Langley support sector and roll mechanism which allowed measurements at angle of attack and at various roll positions.

The data described here is limited to the zero angle of attack and roll case. Other experiments were performed at 4° angle of attack and at various angles around the model. Preliminary tests for pressure distributions and boundary surveys were additionally carried out on a nonconical afterbody model. The results from these tests will be reported in the near future.

VII. MODEL

The tests were made using a model of a typical modern projectile as illustrated in Figure 4. The configuration is an idealization of an artillery projectile consisting of a secant-ogive nose, cylindrical midsection and 7° conical afterbody (boattail) of half a caliber. Turbulent flow was assured by using a sand-grain roughness strip 5 cm from the nose. The 20.2 cm diameter model caused 0.69% blockage of the tunnel which was found acceptable for the measurements carried out. The afterbody was instrumented with 14 static pressure taps located so as to define the flow conditions in the vicinity of the boattail corner.

VIII. INSTRUMENTATION

The boundary layer surveys were made employing the same technique described in Reference 5. The probing mechanism is shown in Figure 5. Some new probe support arms were designed to increase the traversing distance of the probe tip to approximately 30mm. This was found to be necessary on the lee side of the model during the previous tests. Separate probe supports were used to reach the various stations on the model and these were constructed so that all wall pressure tap stations between 3 and 9 (Figure 5) could be investigated. The forward position was expected to be free of the effects of

18. *Reklis, R.P., Danberg, J.E., and Inger, G.R., "Boundary Layer Flows on Transonic Projectiles," AIAA Paper No. 79-1551, AIAA 12th Fluid and Plasma Dynamics Conference, Williamsburg, Viriginia, 1979.*

the expansion at the boattail corner and thus the measurement at this station provides a test of our ability to predict the downstream effects of the boundary layer-shock wave interaction which occurs in the region of the ogive-cylinder junction. The most rearward station, only 1.27 cm from the model base, also provides information about the effects of the afterbody shock wave.

The probe travel is controlled by an electric motor within the model which drives a connecting micrometer lead screw. The control allowed positioning of the probe within ±.03mm. The position of the probe arm was detected using a linearly variable differential transformer which was statically calibrated with an optical cathetometer which provided positioning accuracy of ±0.1mm. The probe tip was electrically insulated so that wall contact provides a reference position for calibration in the tunnel.

A major concern in using total head probes at transonic speeds is the possibility of flow interference; thus, every attempt was made to reduce exposure of the probing mechanism to the main flow field, although some disruption of the base flow is unavoidable. The supersonic region downstream of the boattail corner effectively prevents the upstream propagation of the disturbances caused by the mechanism in wake. This has been verified through photographs of the base flow. No significant upstream effects on the wall static pressure were observed when the probe was in the supersonic region behind the boattail corner. Some upstream propagation from the probe was observed when the probe was in the subsonic flow upstream of the corner, but the disturbance was only significant with the probe tip within one millimeter of the model surface. In all cases the wall static pressure measured without the probe mechanism was used to reduce the Pitot probe pressures to Mach numbers. The Mach number profiles were then reduced to velocity by assuming a Crocco temperature-velocity relationship.

IX. RESULTS

The results of the experimental investigation are summarized in terms of pressure coefficient distributions given in Table 1 and in terms of the boundary layer parameters as given in Table 2. All results shown are for α = 0°, Re = 13 × 10^6/m and M = 0.94 or M = 0.97.

Comparisons between the two theoretical methods and the measurements are made for surface pressure distribution, velocity profiles and displacement thickness. Since no experimental measurements were obtained for skin friction a comparison was made between the two theoretical methods only.

A comparison of the surface pressure coefficient for both computational techniques together with the experimental data for M = 0.94 is shown in Figure 6. The overall agreement is generally quite good. The Navier-Stokes results indicate a better agreement with the experimental data in the vicinity of the expansion (negative C_p peak) but fall off slightly at the last point on the boattail. The computational grid contained only 60 points on the body and was severely stretched in the longitudinal direction after the boattail corner; therefore, the computation may be less accurate in this region. More significant, however, is that the experimental configuration at the base is not fully

15

modeled in the theoretical methods. During the pressure measurements, the probe mechanism is removed, leaving a flat base with a sting of 21% of the base diameter. In contrast, the theoretical solutions are obtained by extending the conical afterbody, thereby approximately accounting for the inviscid flow field but ignoring the free-shear layer and recirculation region near the base. Therefore, agreement between the computation and experiment can not be expected in this region. It should be noted again, however, that the supersonic region on the boattail effectively limits the upstream effects of the base flow.

A difference between the two computed results is seen in the vicinity of the two expansion regions (ogive junction and boattail junction). The upstream influence of the corners is seen to be quite extensive in the Navier-Stokes results, whereas the composite solution is less affected. The composite solution is composed of an inviscid computation which has not been iterated with the boundary layer solution. Therefore, the effect of a boundary layer has not been accounted for in the composite pressure results, whereas the Navier-Stokes results represent a solution of the entire flow field. Additionally, the validity of the Navier-Stokes computation over the entire projectile surface has been shown by Nietubicz[3] to be quite good over a wide Mach number regime.

The sharp spike in pressure coefficient which occurs near the nose tip for the Navier-Stokes results is due to the modeled blunt hemisphere nose shape being computed. Computational experiments, for a hemisphere-cone model of similar bluntness at M = 0.95, have shown that the flow does expand locally to supersonic velocities.

Velocity profiles are shown in Figure 7 for three axial stations at M = 0.94. Stations X/D = 5.36 and 5.61 are from previous test results while the data at X/D = 5.05 has been obtained from the experiment described in this paper. The Navier-Stokes solution (solid line), composite solution (dotted line) and experimental values compare very well in all cases with a slight difference being found for the X/D = 5.36 case. This profile is only .06 caliber downstream from the boattail corner and is therefore in a vicinity of severe expansion. The experimental data were reduced using a constant static wall pressure throughout the boundary layer, which could possibly account for the slight difference in the profile comparison.

A calculation of the displacement thickness was made at all stations where velocity profiles were available. A comparison of the theoretical computations and experimental determination of displacement thickness is shown in Figure 8. The composite solutions show a rapid rise in displacement thickness at the first shock location and then a gradual increase until the expansion of the second corner is felt which then produces a decrease in the displacement thickness. The Navier-Stokes results, on the other hand, show a continuous increase in displacement thickness over the cylinder portion of the model. The experimental results are shown to compare relatively well with the computed values, however, the inability to accurately and consistently determine the boundary layer edge position and velocity in transonic flow makes any comparison suspect. Additionally, the solution of Navier-Stokes equations does not rely on the computation of a displacement surface for improved flow field prediction.

16

Similar comparisons have been made for M = 0.97 in order to determine the applicability of these techniques to Mach number variation. The computed and experimental surface pressure coefficients are again shown in Figure 9 to compare favorably. The velocity profiles at four axial stations for M = 0.97 are shown in Figure 10. The comparison in this case is shown to be good for all stations except X/D = 5.36, which again is in the expansion region. Slightly downstream of the expansion, however, at X/D = 5.49, the agreement is again very good. Station X/D = 5.61 is clearly in the supersonic region at M = 0.97 as evidenced by Schlieren pictures. Disturbances from the probe mechanism are therefore expected to be small in this case. However, for the M = 0.94 case the supersonic pocket is smaller, and interference caused by interaction of the probe and the boattail shock wave is more likely.

Additional features of the computed flow field can be obtained from the Navier-Stokes computations by plotting Mach = 1 contour line. Figure 11 is a composite picture showing the computed contours together with a Schlieren photograph of the boattail region. The photograph is a composite itself of two Schlieren pictures. The upstream region was obtained by translating the model 8" downstream in order to bring the ogive-cylinder junction shock wave into view of the camera. Although the wave locations can only be determined within a small region because of optical effects, the results are generally consistant but slightly forward of the predicted Mach one lines. The relative movement of the shock waves between M = 0.94 and M = 0.97 is consistant with the theoretical prediction.

A usually severe test of the computational capability is the accurate prediction of the skin friction coefficient. Although the experimental data have not been reduced for comparison, Figure 11 does show the results for both numerical schemes. The expansion about both corners is shown to produce a rapid increase in the skin friction followed by a rapid decrease after the shock. The relative agreement between these two methods, especially in the presence of multiple shocks, is considered to be quite good.

X. CONCLUSION

The transonic flow field about a secant-ogive-cylinder-boattailed model has been computed using a generalized axisymmetric Navier-Stokes code and a composite shock boundary layer interaction technique. The computations have been compared to the experimental data at M = 0.94 and 0.97 for α = 0. The results show generally good agreement considering the complex double-shock environment such as exists about this projectile shape.

Additional experimental data is required to fully assess the validity of the computational techniques; however, comparison of the two computational methods with the available data shows generally good agreement. The velocity profile comparisons are exceptionally good considering the severe expansion occurring at the boattail corner. The expansion and recompression areas are apparent from the C_p curves and the agreement with the data for surface pressure is especially good. A refined grid near the boattail base should improve the Navier-Stokes results in that area.

Navier-Stokes computations have been obtained for the projectile shape considered here at angle of attack, and comparisons of these results with the available experimental data and the composite solution technique will be reported in the future.
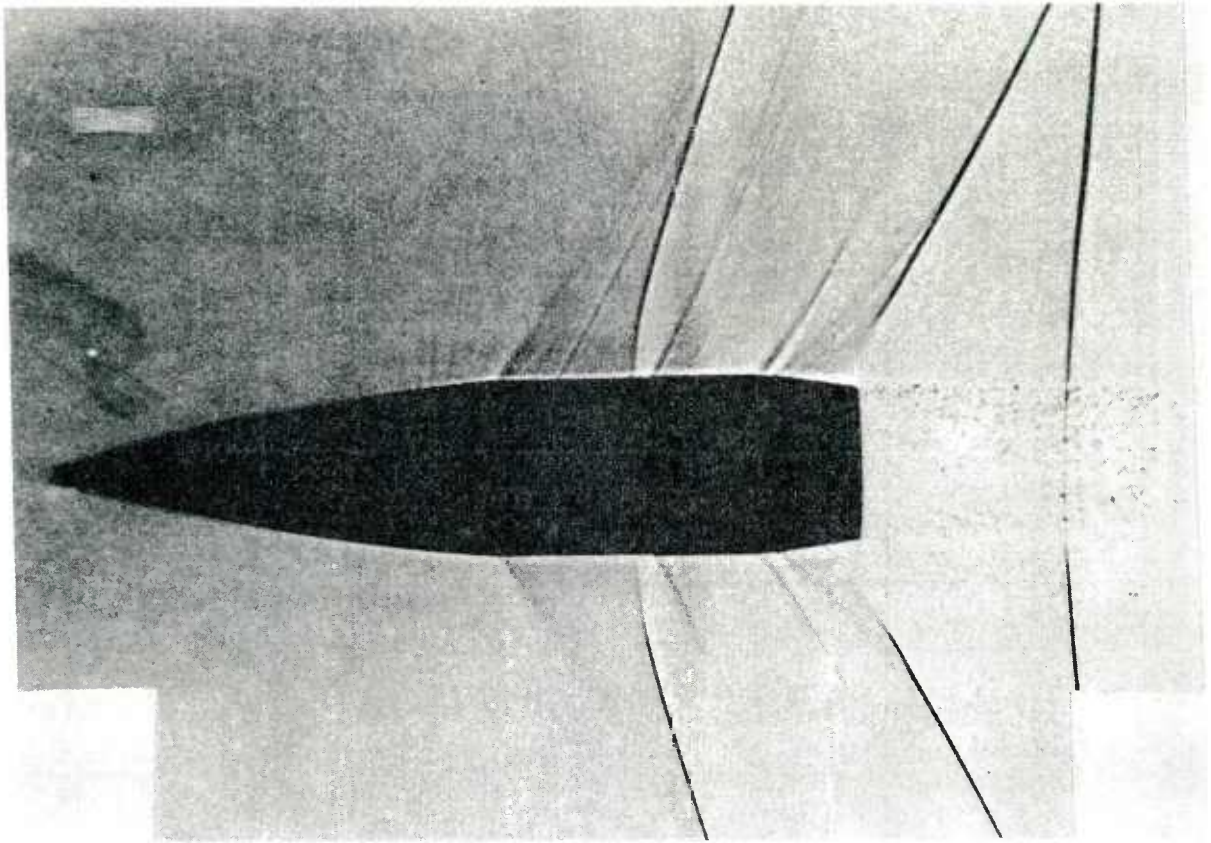
ACKNOWLEDGEMENT

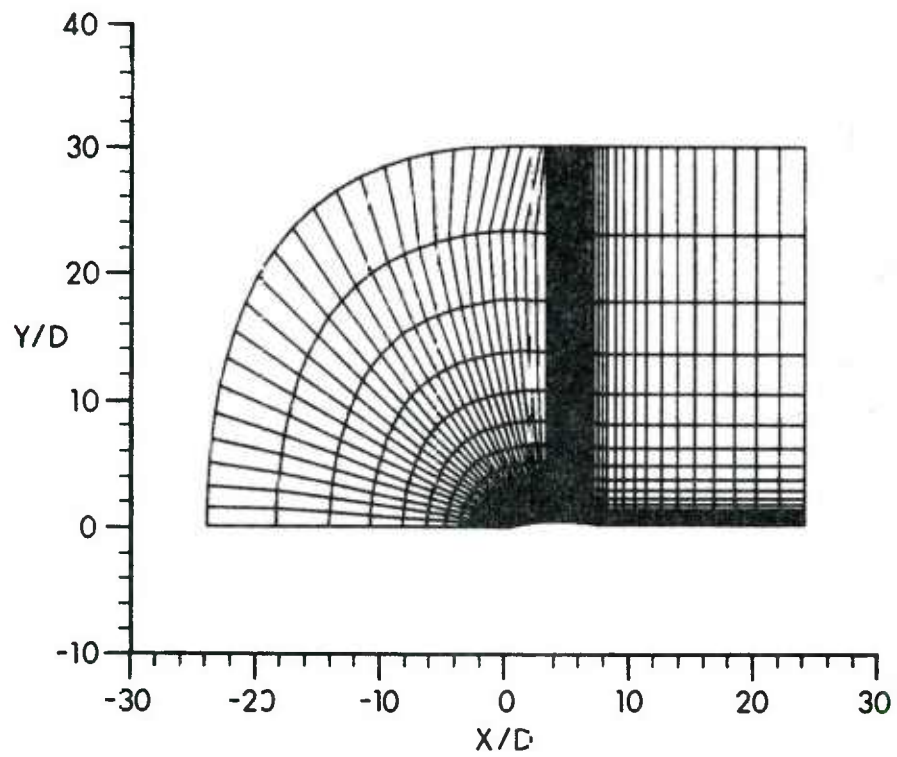Figure 1. Spark Shadowgraph of Projectile at Transonic Velocity, M ≈ .98

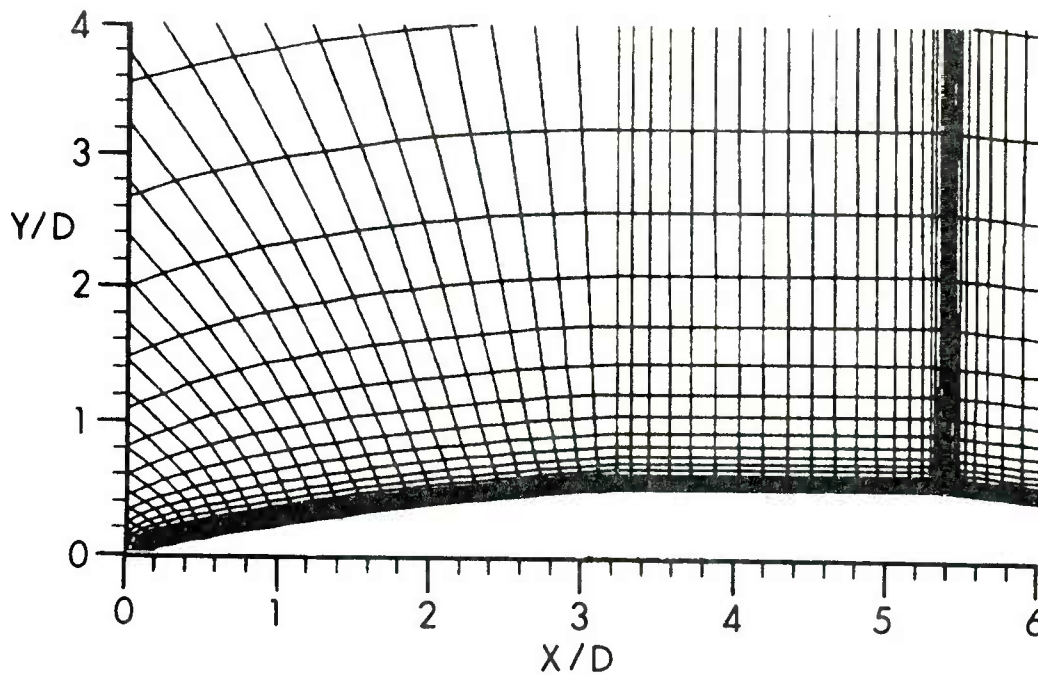Figure 2a. Physical Grid for Navier-Stokes Computations - Full Grid

Figure 2b.   Physical Grid for Navier-Stokes Computations
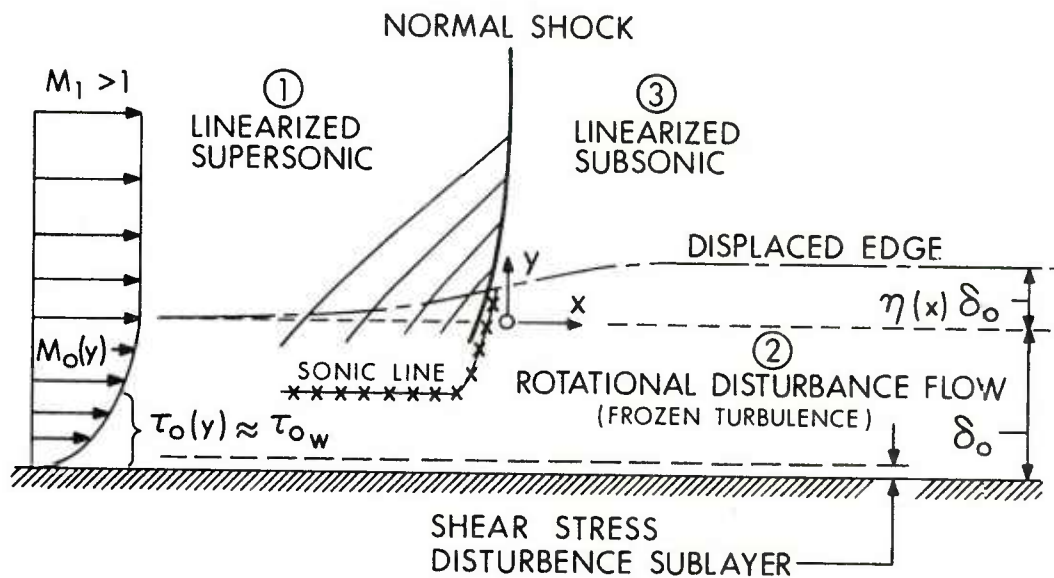- Expanded View Near Model

Figure 3.   Triple Deck Model of Shock Boundary Layer Interaction
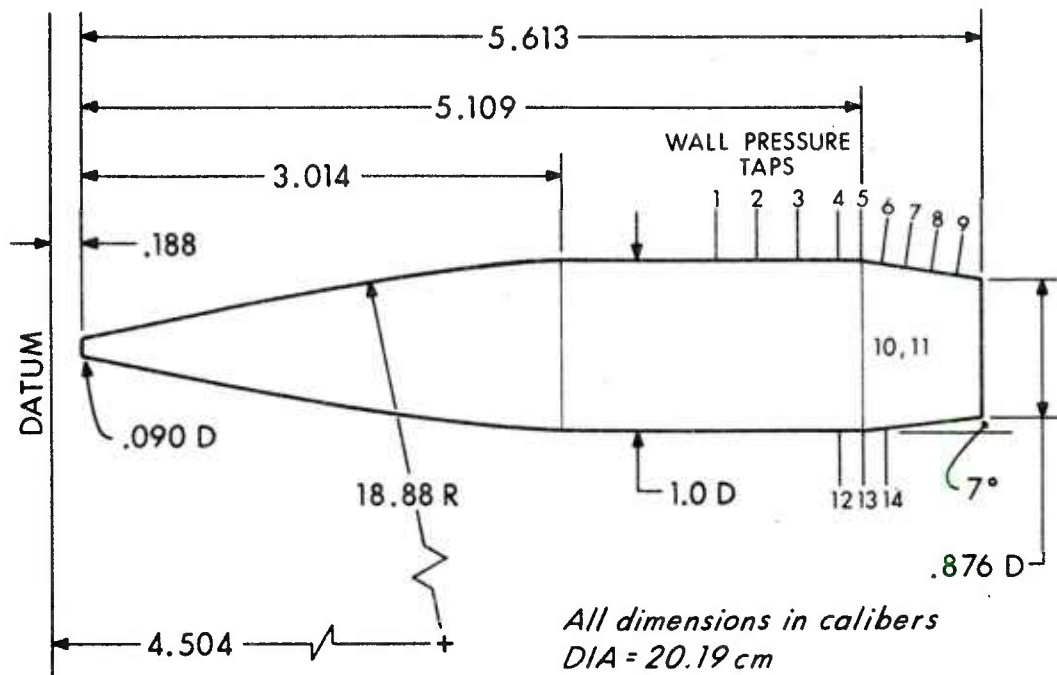
20

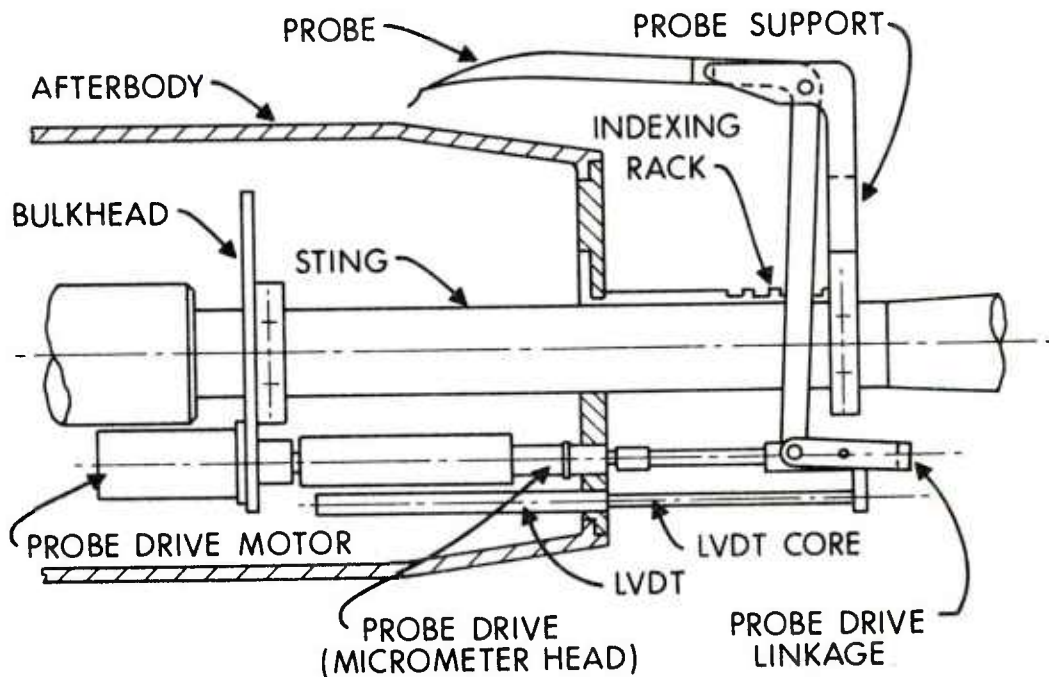Figure 4. Boattailed Model Configuration

Figure 5. Afterbody of Wind Tunnel Model Showing Probe Support Mechanism

21

Figure 6. Comparison of Navier-Stokes, Composite and Experimental
Surface Pressure Coefficients, M = 0.94
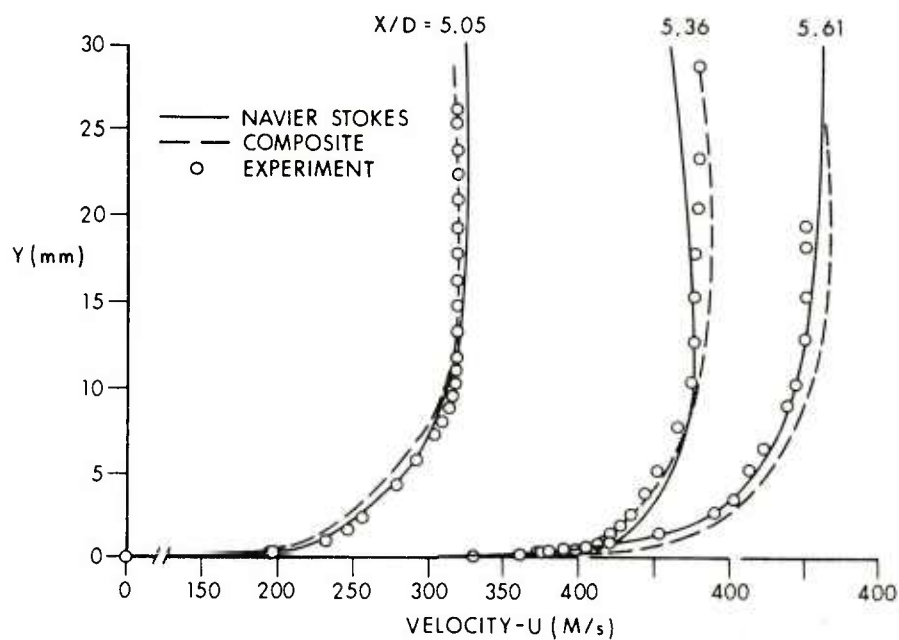
Figure 7. Velocity Profiles at X/D = 5.05, 5.36 and 5.61 for M = 0.94, $\alpha = 0°$
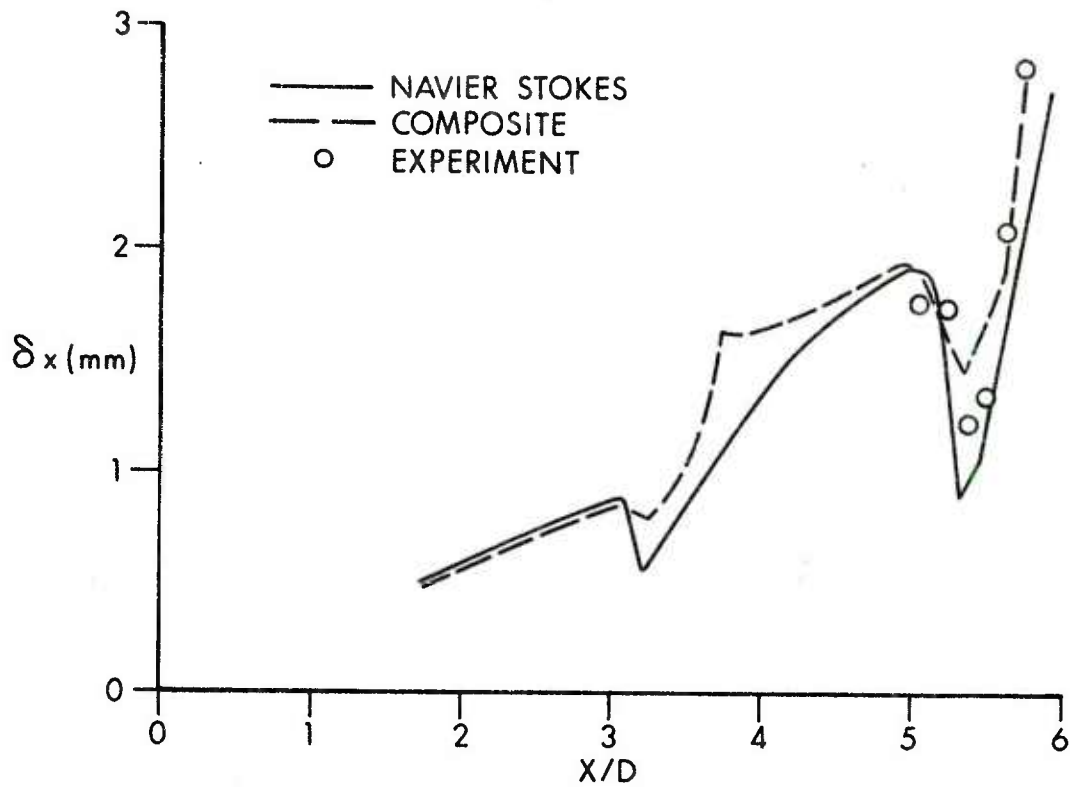
Figure 8. Comparison of Displacement Thicknesses: Experiment, Navier-Stokes and Composite, M = 0.94, α = 0°
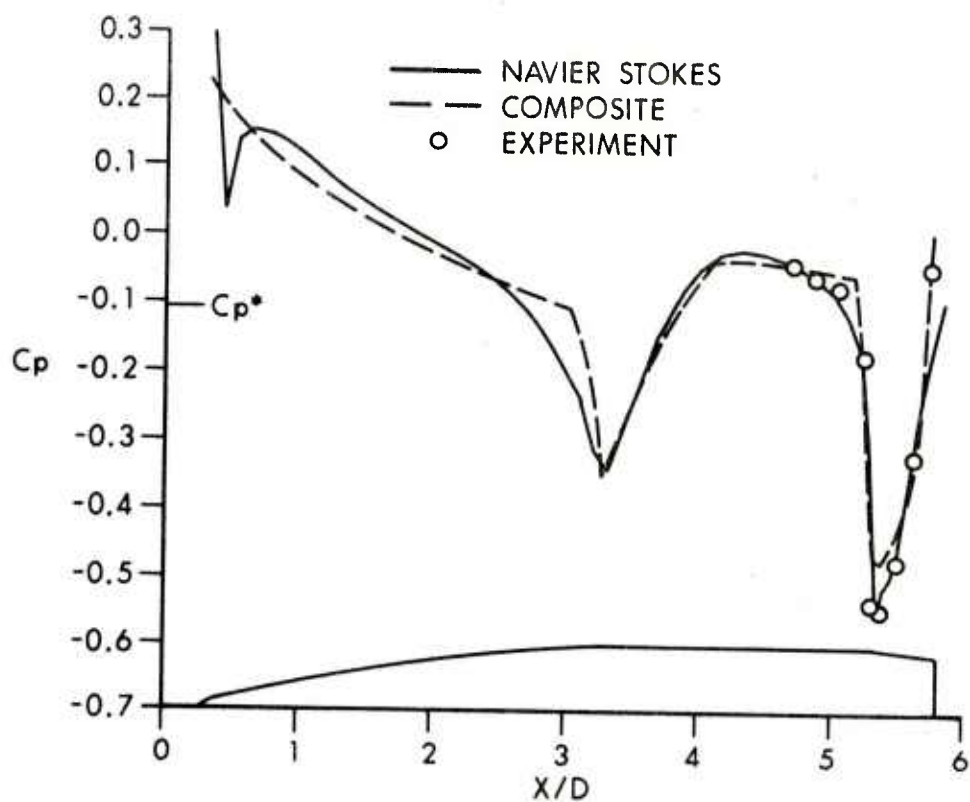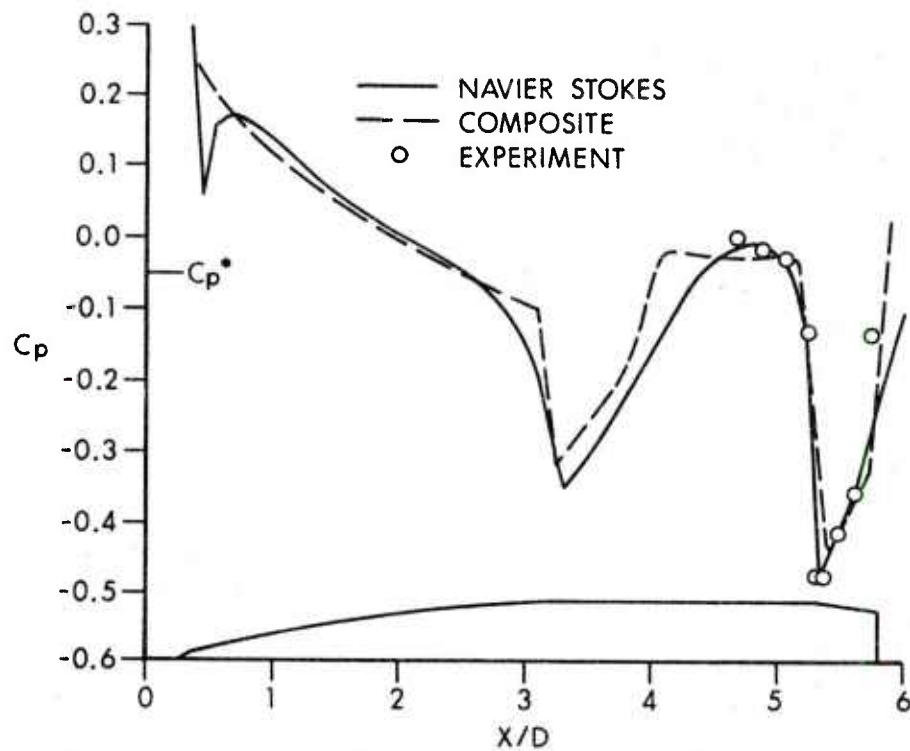

Figure 9. Comparison of Navier-Stokes, Composite and Experimental Surface Pressure Coefficients, M = 0.97, α = 0°

23
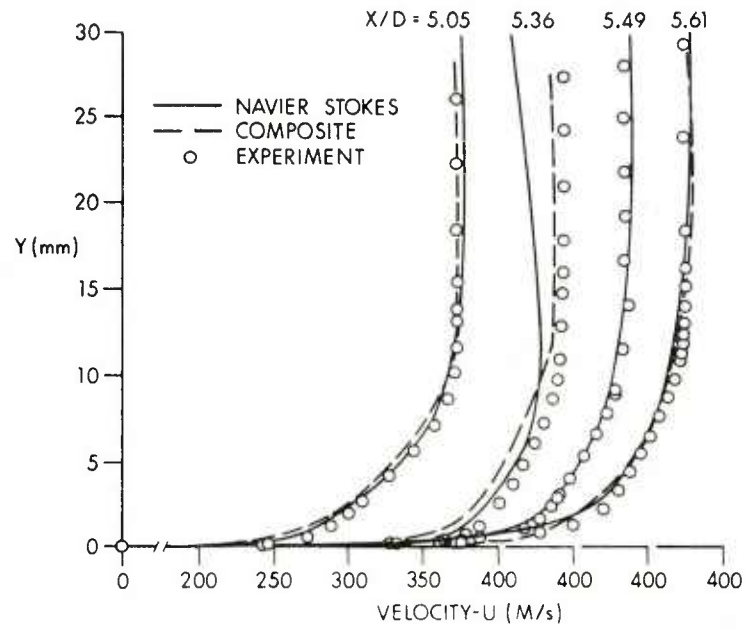
Figure 10. Velocity Profiles at X/D = 5.05, 5.36, 5.49 and 5.61 for M = 0.97, α = 0°
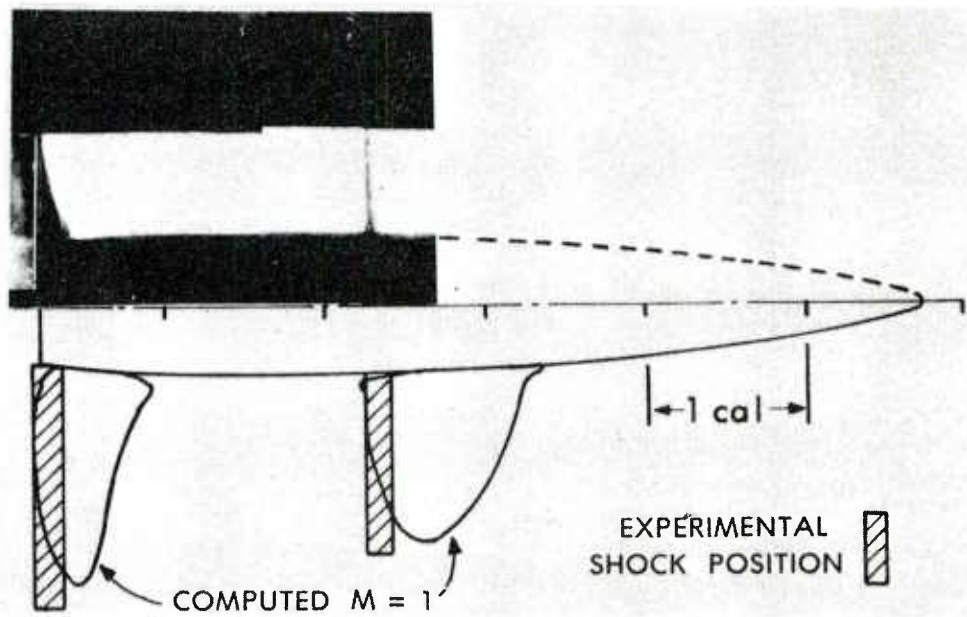
Figure 11. Boattail Shock Formation from Computer Mach Number Contours and Schlieren Photo
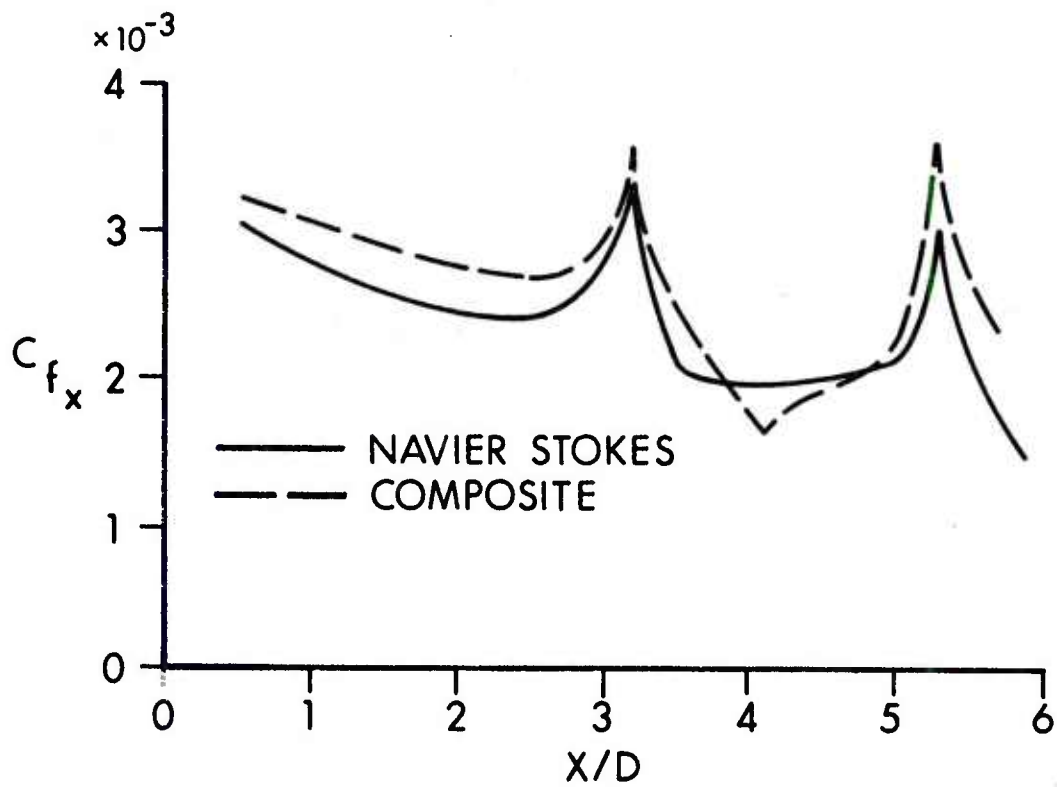
Figure 12. Comparison of Skin Friction Coefficient Between Navier-Stokes and Composite Solution Technique M = 0.97, α = 0°

TABLE 1. EXPERIMENTAL AFTERBODY PRESSURE DISTRIBUTION $\alpha = 0°$

$M_\infty =$		0.94	0.97
TAP	X/L	Cp	Cp
1	.805	-.040	.000
2	.837	-.054	-.014
3	.870	-.068	-.029
12	.891	-.107	-.063
4	.902	-.165	-.127
5	.913	-.535	-.478
6	.924	-.542	-.478
14	.935	-.505	-.439
7	.946	-.472	-.413
8	.967	-.314	-.345
9	.989	-.036	-.106
10	.913	-.523	-.464
11	.913	-.561	-.497
13	.913	-.561	-.439
BASE		-.004	-.005

TABLE 2. MEASURED BOUNDARY LAYER CHARACTERISTICS $\alpha = 0°$

X/L	δ mm	δ^*_X mm	θ_X mm	H_X
$M_\infty = 0.94$				
.869	10.94	1.74	.99	1.75
.902	11.53	1.68	.97	1.73
.924	13.22	1.33	.75	1.78
.946	11.57	1.39	.74	1.88
.968	12.59	2.05	1.07	1.92
.989	13.97	2.79	1.44	1.94
$M_\infty = 0.97$				
.869	10.94	1.81	1.02	1.77
.924	16.45	1.47	.78	1.88
.946	11.46	1.48	.78	1.90
.968	11.82	1.68	.88	1.91
.989	12.71	2.32	1.22	1.90

NOTE: a). δ based on $u/u_e = 0.995$.

b). δ^*_X and θ_X based on 2-D definitions

$$\delta^*_X = \int_0^\delta \left(1 - \frac{\rho u}{\rho_e u_e}\right) \, dy$$

$$\theta_X = \int_0^\delta \frac{\rho u}{\rho_e u_e} \left(1 - \frac{u}{u_e}\right) \, dy$$

$$H_X = \delta^*_X / \theta_X$$

REFERENCES

1. Sturek, W.B., et al., "Computations of Magnus Effects for a Yawed, Spinning Body of Revolution," <u>AIAA Journal</u>, Vol. 16, No. 7, July 1978, pp. 687-692.

2. Schiff, L.B., and Sturek, W.B., "Numerical Simulation of Steady Supersonic Flow Over an Ogive-Cylinder-Boattail Body," AIAA Paper No. 80-0066, January 14-16, 1980.

3. Nietubicz, C.J., "Navier-Stokes Computations for Conventional and Hollow Projectile Shapes at Transonic Velocities," AIAA Paper No. 81-1262, AIAA 14th Fluid and Plasma Dynamics Conference, Palo Alto, CA, 1981.

4. Reklis, R.P., Sturek, W.B., and Bailey, F.L., "Computation of Transonic Flow Past Projectiles at Angle of Attack," U.S. Army Ballistic Research Laboratory, ARRADCOM, Aberdeen Proving Ground, MD, Technical Report ARBRL-TR-02139, February 1979 (AD 069106).

5. Danberg, J.E., Reklis, R.P., and Inger, G.R., "Pressure Distributions and Boundary Layer Profiles on a Yawed Projectile at Transonic Speeds," University of Delaware Tech Report No. 226, Department of Mechanical and Aerospace Engineering, April 1979.

6. Deiwert, G.S., "Numerical Simulation of Three-Dimensional Boattail Afterbody Flow Field," AIAA Paper No. 80-1347, July 1980.

7. Nietubicz, C.J., Pulliam, T.H., and Steger, J.L., "Numerical Solution of the Azimuthal-Invariant Thin-Layer Navier-Stokes Equations," <u>AIAA Journal</u> Vol. 18, No. 12, December 1980, pp. 1411-1412.

8. Pulliam, T.H., and Steger, J.L., "On Implicit Finite-Difference Simulations of Three-Dimensional Flow," <u>AIAA Journal</u>, Vol. 18, No. 2, February 1980, pp. 159-167.

9. Baldwin, B.S., and Lomax, H., "Thin Layer Approximation and Algebraic Model for Separated Turbulent Flows," AIAA Paper No. 78-257, January 1978.

10. Beam, R., and Warming, R.F., "An Implicit Factored Scheme for the Compressible Navier-Stokes Equations," AIAA Paper No. 77-645, June 1977.

11. Steger, J.L., Nietubicz, C.J., and Heavey, K.R., "A General Curvilinear Grid Generation Program for Projectile Configurations," ARBRL-MR-03142, U.S. Army Ballistic Research Laboratory, ARRADCOM, Aberdeen Proving Ground, MD 21005, March 1982 (AD A107334).

12. Dwyer, H.A., and Sanders, B.R., "Magnus Forces on Spinning Supersonic Cones. Part I. The Boundary Layer," <u>AIAA Journal</u>, Vol. 14, April 1976, p. 498.

REFERENCES (Cont'd)

13. Inger, G.R., "Upstream Influence and Skin Friction of Non-Separating Shock-Turbulent Boundary Layer Interaction," AIAA Paper 80-1411, Snowmass, CO, July 1980.

14. Stanewsky, E., Nanandan, M., and Inger, G.R., "Computation of Transonic Flow on Supercritical Airfoils with a Special Solution for Shock-Boundary Layer Interaction," in AGARD CP-291 ("Computation of Viscous-Inviscid Interactions"), September 1980.

15. Inger, G.R., "Transonic Shock-Turbulent Boundary Layer Interactions on Spinning Axisymmetric Bodies at Zero Angle of Attack," ARBRL-TR-02458, U.S. Army Ballistic Research Laboratory, ARRADCOM, Aberdeen Proving Ground, MD 21005, January 1983 (AD A123389).

16. Murman, E.M., and Cole, J.D., "Calculation of Plane Steady Transonic Flow," AIAA Journal, Vol. 9, No. 1, January 1971, pp. 114-121.

17. Walz, A., "Boundary Layers of Flow and Temperature," M.I.T. Press, Cambridge, MA, 1969, p. 113.

18. Reklis, R.P., Danberg, J.E., and Inger, G.R., "Boundary Layer Flows on Transonic Projectiles," AIAA Paper 79-1551, AIAA 12th Fluid and Plasma Dynamics Conference, Williamsburg, Virginia, 1979.

DISTRIBUTION LIST

No. of Copies	Organization	No. of Copies	Organization
12	Administrator Defense Technical Info Center ATTN: DTIC-DDA Cameron Station Alexandria, VA 22314	1	Director US Army Air Mobility Research and Development Laboratory Ames Research Center Moffett Field, CA 94035
1	Commander US Army Materiel Development and Readiness Command ATTN: DRCDMD-ST 5001 Eisenhower Avenue Alexandria, VA 22333	1	Commander US Army Communications Rsch and Development Command ATTN: DRSEL-ATDD Fort Monmouth, NJ 07703
8	Commander US Army Armament Research and Development Command ATTN: DRDAR-TDC DRDAR-TSS DRDAR-LCA-F Mr. D. Mertz Mr. A. Loeb Mr. S. Wasserman Mr. H. Hudgins Mr. E. Friedman Dover, NJ 07801	1	Commander US Army Electronics Research and Development Command Technical Support Activity ATTN: DELSD-L Fort Monmouth, NJ 07703
		2	Commander US Army Missile Command ATTN: DRSMI-R DRSMI-RDK Mr. R. Deep Redstone Arsenal, AL 35898
1	Commander US Army Armament Materiel Readiness Command ATTN: DRSAR-LEP-L Rock Island, IL 61299	1	Commander US Army Missile Command ATTN: DRSMI-YDL Redstone Arsenal, AL 35898
1	Director US Army Armament Research and Development Command Benet Weapons Laboratory ATTN: DRDAR-LCB-TL Watervliet, NY 12189	1	Commander US Army Tank Automotive Command ATTN: DRSTA-TSL Warren, MI 48090
1	Commander US Army Aviation Research and Development Command ATTN: DRDAV-E 4300 Goodfellow Blvd. St. Louis, MO 63120	1	Director US Army TRADOC Systems Analysis Activity ATTN: ATAA-SL White Sands Missile Range NM 88002
		1	Commander US Army Research Office P. O. Box 12211 Research Triangle Park NC 27709

DISTRIBUTION LIST

No. of Copies	Organization
1	Commander US Naval Air Systems Command ATTN: AIR-604 Washington, D. C. 20360

4	Commander
	US Naval Surface Weapons
	  Center
	ATTN: Dr. T. Clare, Code DK20
	    Dr. P. Daniels
	    Mr. D. A. Jones III
	    Mr. L. Mason
	Dahlgren, VA 22448

4	Commander
	US Naval Surface Weapons
	  Center
	ATTN: Code 312
	    Dr. C. Hsieh
	    Dr. W. Yanta
	    Mr. R. Voisinet
	    Code R44
	    Dr. R. U. Jettmar
	Silver Spring, MD 20910

1	Commander US Naval Weapons Center ATTN: Code 3431, Tech Lib China Lake, CA 93555
1	Director NASA Langley Research Center ATTN: NS-185, Tech Lib Langley Station Hampton, VA 23365
2	Commandant US Army Infantry School ATTN: ATSH-CD-CSO-OR Fort Benning, GA 31905

3	Director
	NASA Ames Research Center
	ATTN: MS-202A-14, Dr. P. Kutler
	    MS-202-1, Dr. T. Pulliam
	    MS-227-8, Dr. L. Schiff
	Moffett Field, CA 94035

No. of Copies	Organization

2	Sandia Laboratories
	ATTN: Division No. 1331,
	    Mr. H.R. Vaughn
	    Mr. G.R. Eisler
	P.O. Box 580
	Albuquerque, NJ 87115

1	AEDC Calspan Field Services ATTN: MS 600 (Dr. John Benek) AAFS, TN 37389
1	Stanford University Department of Aeronautics and Astronautics ATTN: Prof. J. Steger Stanford, CA 94035

1	University of California,
	  Davis
	Department of Mechanical
	  Engineering
	ATTN: Prof. H.A. Dwyer
	Davis, CA 95616

1	University of Delaware Mechanical and Aerospace Engineering Department ATTN: Dr. J. E. Danberg Newark, DE 19711
1	Dr. George R. Inger Associate Chairman, Dept. of Mech. & Aero. Engr. West Virginia University Morgantown, W. VA 26506

Aberdeen Proving Ground

Dir, USAMSAA
  ATTN: DRXSY-D
    DRXSY-MP, H. Cohen

Cdr, USATECOM
  ATTN: DRSTE-TO-F

Dir, USACSL, Bldg. E3516, EA
  ATTN: DRDAR-CLB-PA
    DRDAR-CLN
    DRDAR-CLJ-L

USER EVALUATION OF REPORT

Please take a few minutes to answer the questions below; tear out this sheet, fold as indicated, staple or tape closed, and place in the mail. Your comments will provide us with information for improving future reports.

1. BRL Report Number _____

2. Does this report satisfy a need? (Comment on purpose, related project, or other area of interest for which report will be used.)

_____

_____

_____

3. How, specifically, is the report being used? (Information source, design data or procedure, management procedure, source of ideas, etc.) _____

_____

_____

4. Has the information in this report led to any quantitative savings as far as man-hours/contract dollars saved, operating costs avoided, efficiencies achieved, etc.? If so, please elaborate.

_____

_____

5. General Comments (Indicate what you think should be changed to make this report and future reports of this type more responsive to your needs, more usable, improve readability, etc.) _____

_____

_____

_____

6. If you would like to be contacted by the personnel who prepared this report to raise specific questions or discuss the topic, please fill in the following information.

Name: _____

Telephone Number: _____

Organization Address: _____

_____

_____